NANO LETTERS

Letter

pubs.acs.org/NanoLett

Atom-by-Atom Observation of Grain Boundary Migration in Graphene

Simon Kurasch,[†,¶] Jani Kotakoski,*[,‡,§,¶,●] Ossi Lehtinen,[‡,¶,●] Viera Skákalová,[∥,■] Jurgen Smet,[∥] Carl E. Krill, III,[⊥] Arkady V. Krasheninnikov,[‡,#] and Ute Kaiser*[,†]

[†]Central Facility for Electron Microscopy, Group of Electron Microscopy of Materials Science, Ulm University, 89081 Ulm, Germany

[‡]Department of Physics, University of Helsinki, P.O. Box 43, 00014 Helsinki, Finland

[§]Department of Physics, University of Vienna, Boltzmanngasse 5, 1090 Vienna, Austria

[∥]Max Planck Institute for Solid State Research, Heisenbergstrasse 1, 70569 Stuttgart, Germany

[⊥]Institute of Micro and Nanomaterials, Ulm University, Albert-Einstein-Allee 47, 89081 Ulm, Germany

[#]Department of Applied Physics, Aalto University, P.O. Box 1100, 00076 Aalto, Finland

Supporting Information

ABSTRACT: Grain boundary (GB) migration in polycrystalline solids is a materials science manifestation of survival of the fittest, with adjacent grains competing to add atoms to their outer surfaces at each other's expense. This process is thermodynamically favored when it lowers the total GB area in the sample, thereby reducing the excess free energy contributed by the boundaries. In this picture, a curved boundary is expected to migrate toward its center of curvature with a velocity proportional to the local radius of boundary curvature (R). Investigating the underlying mechanism of boundary migration in a 3D material, however, has been reserved for computer simulation or analytical theory, as capturing the dynamics of individual atoms in the core region of a GB is well beyond the spatial and temporal resolution limits of current characterization techniques. Here, we similarly overcome the conventional experimental limits by investigating a 2D material, polycrystalline graphene, in an aberration-corrected transmission electron microscope, exploiting the energy of the imaging electrons to stimulate individual bond rotations in the GB core region. The resulting morphological changes are followed in situ, atom-by-atom, revealing configurational fluctuations that take on a time-averaged preferential direction only in the presence of significant boundary curvature, as confirmed by Monte Carlo simulations. Remarkably, in the extreme case of a small graphene grain enclosed within a larger one, we follow its shrinkage to the point of complete disappearance.

KEYWORDS: *Graphene, transmission electron microscopy, grain boundaries, Monte Carlo, transformation, migration*

Adjacent grains in polycrystalline graphene are separated by tilt boundaries. The low-energy configurations of these GBs consist of arrangements of pentagon−heptagon (5|7) pairs[1−3] with a width below 1 nm, whereas the pristine lattice consists of only hexagonal carbon rings. In contrast to the GBs in most bulk materials, the atomic density in graphene GBs is typically nearly the same as that of the adjacent crystallites (i.e., zero or nearly zero density deficit), likely owing to the strongly covalent bonding between atoms and the energy penalty associated with dangling bonds. The graphene samples used in our study were grown by the chemical vapor deposition technique (Methods) on polycrystalline Cu foils. After growth, the graphene membranes were transferred to commercial TEM grids for electron beam-stimulated modification and simultaneous aberration-corrected high-resolution transmission electron microscopy (AC-HRTEM) imaging in an FEI Titan 80−300 microscope operated at 80 kV (Methods).

An overview of our sample is presented in Figure 1. As can be seen in both the HRTEM image (Figure 1a) and the lower-magnification dark-field image (Figure 1b), the specimen is highly polycrystalline. Even though graphene is known to grow nonepitaxially on Cu,[4] the distribution of misorientation angles between adjacent grains (inset, Figure 1a) reveals a strong propensity for neighboring grains to be misoriented by $\theta \approx 30°$. This is because, in contrast to earlier reports,[5] our sample contains a significant fraction of small grains enclosed within larger ones for which this misorientation is the lowest-energy crystallographic configuration. As expected, the observed GBs are predominantly constructed of continuous chains of (5|7) pairs and, similar to previous observations,[5−7] the GBs tend to take on meandering, locally curved configurations. These shapes reduce the lattice strain that would result from straight boundaries separating randomly oriented grains, and which could, in turn, cause buckling of the membrane.[2]

Significant changes in the atomic structure of graphene can be induced via bond rotations under 80 kV electron irradiation, as we have previously shown.[8,9] Although electron irradiation at 80 kV can displace atoms from edges of holes in graphene,[10] knock-on sputtering of three-coordinated carbon atoms becomes significant only at slightly higher voltages, as is extensively explained in ref 11. Correspondingly, hole growth in graphene under 80 kV electron irradiation is driven by chemical effects, not knock-on displacements.[11] Such irradiation will also

Received: March 24, 2012
Revised: April 19, 2012
Published: May 3, 2012

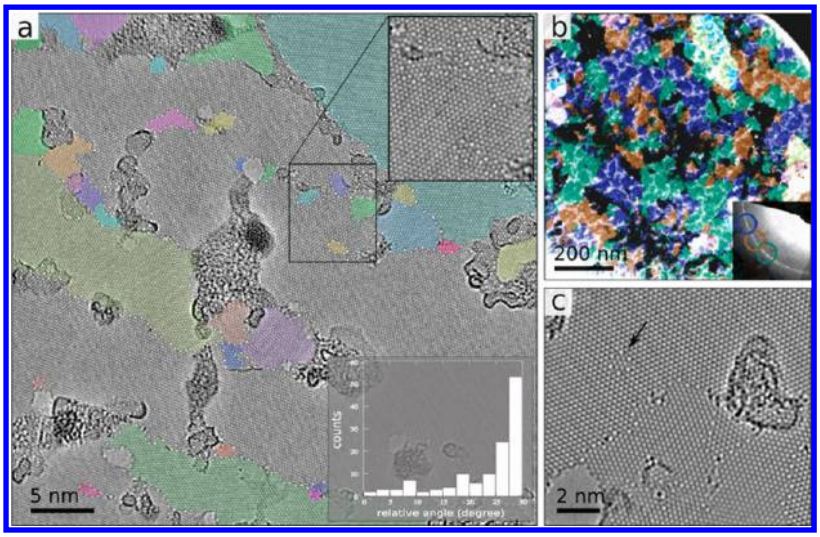

Figure 1. Overview of the graphene sample. (a) HRTEM image with individual grains shaded in color. Insets show a higher magnification of the area marked in the image and the distribution of misorientation angles between adjacent grains, as measured from similar HRTEM images. (b) False-color dark-field image providing a wider view of the sample. The various colors correspond to the different orientations indicated in the diffraction pattern (inset). (c) Higher-magnification HRTEM image featuring several GBs and a small flowerlike grain[17] (arrow) embedded in a larger one.

cause only slight heating of the sample.[12] At voltages below 80 kV, bond rotations are too scarce to lead to significant configurational changes[5] (the lower the voltage, the fewer bond rotations per unit time). Therefore, by exposing graphene to 80 keV electrons, we deliberately maximize the bond rotation rate, resulting in measurable changes in graphene GB morphology during the time scale of a typical experiment in the electron microscope. In the case of straight twin boundaries, the GB energy per unit length (γ) has already been shown to depend primarily on the misorientation angle θ.[1−3] According to our density functional theory (DFT) calculations (Methods), this remains true also for more realistic, serpentine GB configurations (for $\theta \approx 30°$ all γ are within 0.03 eV/Å, the absolute value being an order of magnitude higher). Therefore, the driving force (per unit GB length) for migration of a given GB between two grains, γ/R,[13] should depend only on its local in-plane curvature and not on its detailed atomic structure. Hence, at low boundary curvature ($R \rightarrow \infty$) there is no preferred direction of migration, whereas in the high-curvature limit ($R \rightarrow 0$) the driving force should favor decreasing the GB length and thereby shrinking the grain located on the same side of the boundary as the center of curvature. The decrease of GB length in a 2D material is analogous to decrease of GB area in conventional 3D materials.

We first consider the behavior of boundaries between larger grains in the sample. The GB shown in Figure 2 terminates at two holes that formed under the electron beam as a result of electron beam-induced chemical etching[14] occurring at adsorbates attached to the GB outside our area of interest. Such holes grow steadily during a TEM experiment[14−16] and they might pin the ends of the GB, preventing its migration beyond the pore edges, similar to the Zener-pinning effect in conventional materials.[17] As indicated schematically in Figure 2, the boundary is constructed of a continuous chain of (5|7) pairs interspersed occasionally with distorted hexagons, which similarly serve as dislocation cores in the graphene lattice.[8] The misorientation angle between the grains is close to 30°. As expected, upon continuous irradiation we observe the boundary structure to undergo sequential bond rotations in the series of micrographs recorded during an 11 min exposure (Figure 2a−h). Since the driving force for GB migration is negligible at large R, the boundary fluctuates between different shapes around a more-or-less straight configuration, with no favored direction for GB translation. Longer image sequences of such transformations are presented in the Supporting Information Videos 1 and 2.

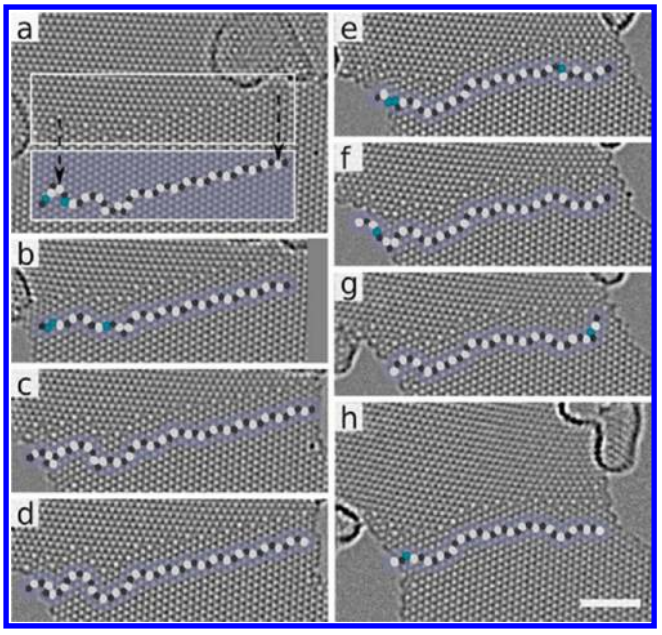

Figure 2. Bond rotation-mediated configurational changes of a graphene GB with low overall curvature. The image sequence shows the same GB during prolonged electron beam exposure (11 min between panels a and h at an approximate dose rate of 1.0×10^6 e/(nm^{2}s)). As indicated in the boxed region in panel a, the GB structure is drawn schematically beneath each boundary image, with pentagons shaded black and heptagons white. Distorted hexagons (cyan) take the place of (5|7) pairs at locations of apparent discontinuities in the GB. Scale bar is 2 nm.

Next, we direct our attention to smaller grains (~1−2 nm) for which the driving force associated with boundary curvature is expected to become significant. To gain a better under-

dx.doi.org/10.1021/nl301141g | Nano Lett. 2012, 12, 3168−3173

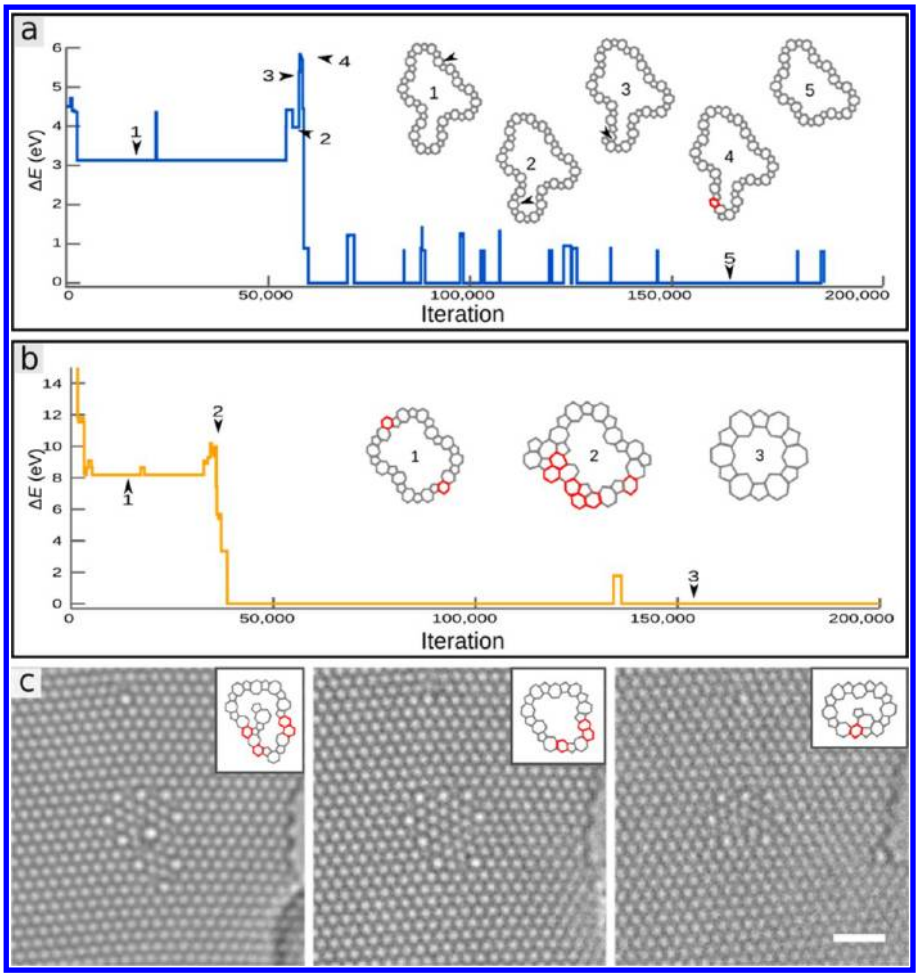

Figure 3. Migration of boundaries surrounding small grains. (a,b) Two examples from MC simulations at simulation temperatures of 2500 K (a) and 2000 K (b) in which an initially larger grain transforms into a smaller one via sequential bond rotations in the GB core. The graphs show the total energy of each of the systems relative to that of the final structure reached during the simulation. In panel (a), the rotating bonds associated with overcoming the barrier are marked with arrows in structures 1−3. (c) A sequence of micrographs showing the shrinkage of a small grain during imaging with an electron beam at a dose rate of approximately 8.7×10^6 e/(nm^{2}s) during a 9 min exposure. Insets show schematically the GB structure in each micrograph. Scale bar 1 nm.

standing of the effect of bond rotations on the energetics and boundary kinetics of small grains, we developed a Metropolis Monte Carlo (MC) code utilizing an analytical interaction model[18] (see Methods and Supporting Information for further details). This code allows us to find low-energy transformation routes between different structures connected by a sequence of individual bond rotations. We first created several graphene grains having sizes comparable to those observed experimentally and then studied how bond rotations changed the atomic configurations and total energy at each stage of structural transformation. In Figure 3a,b, we present two examples from our simulations. In both cases, the initial structure rapidly reaches a local equilibrium configuration. However, further reduction in energy takes place only after an energy barrier has been overcome, which requires several bond rotations to occur in sequence, each of which increases the energy of the simulation structure. Under our experimental conditions, such steps can occur only with assistance from the electron beam (the thermal activation rate for bond rotation is extremely low at room temperature, as the required energy is 6−10 eV[19]). However, this energy input is more than recovered on the other side of the barrier, thus making the reverse process much less likely.

The simulated atomic configuration presented in Figure 3b eventually transforms into a flowerlike structure.[20,21] This hexagon-shaped grain (flower defect) has been reported previously in both nitrogen-doped[20,21] and pristine graphene.[22,23] Interestingly, a similar structure can form from carbon adsorbates on graphene substrates at high temperatures.[24] It is also the single most prevalent grain structure observed in our samples. This particular boundary configuration can be created via six consecutive bond rotations. As noted above, the reverse transformation is unlikely, owing to a considerable energy barrier (circa 8 eV according to the analytical interaction model). Clearly, unlike the reversible changes observed for boundaries with large R, the driving force associated with high-boundary curvature can lead to irreversible shrinkage of smaller grains. The configurational transformations generated by the MC simulations are validated by similar transformations recorded under the electron microscope. One example is shown in Figure 3c (more frames are available in Supporting Information Video 3) and another one in Figure 4d.

When the shrinkage of small grains having zero density deficit is taken to its logical conclusion, one could expect to observe the complete disappearance of these structures. This is indeed possible, as we demonstrate in Figure 4a, which shows

dx.doi.org/10.1021/nl301141g | Nano Lett. 2012, 12, 3168−3173

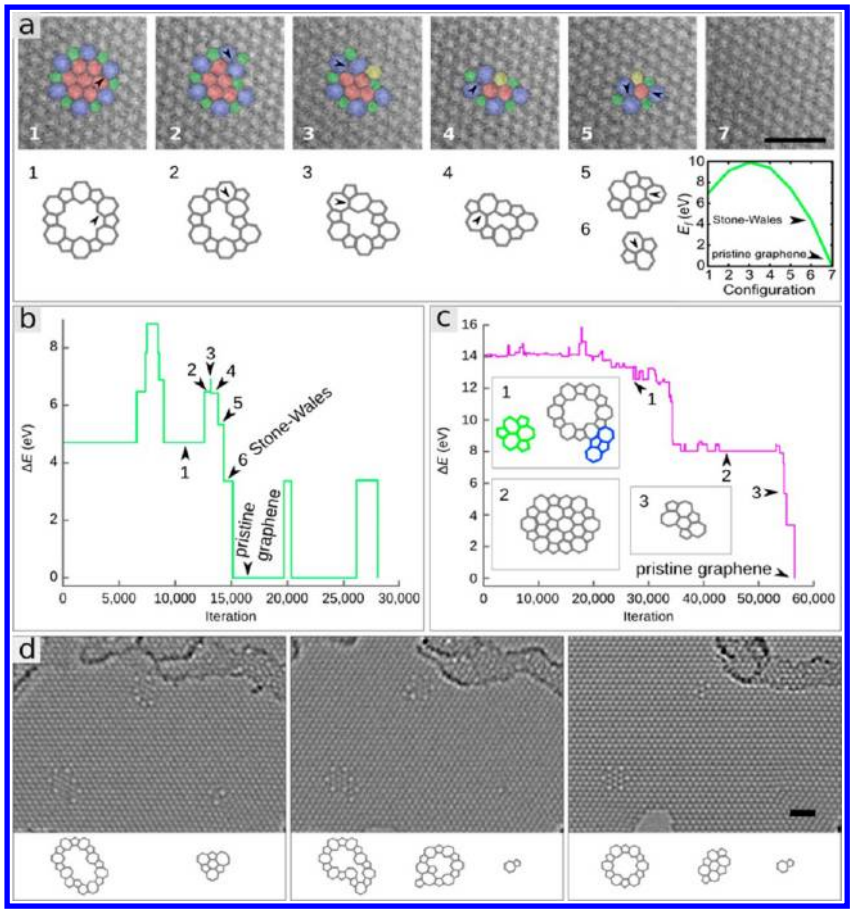

Figure 4. "Unwinding" the flower defect and an example of configurational changes of boundaries with nonzero density deficit. (a) A sequence of micrographs showing the disappearance of a flower defect under an electron flux of approximately 1.0×10^7 e/(nm^{2}s) during a 30 s total exposure (micrographs without overlays are presented in Supporting Information Figure 1 and frames with a larger field of view are presented as Supporting Information Video 4). Each intermediate stage of the unwinding process is captured here except for the last one, number 6, the Stone-Wales defect, before pristine graphene is reached. Below the experimental images are DFT-optimized models of the same structures and a plot of their formation energies. Rotating bonds are indicated by black arrows. (b) Evolution of the total energy of an unwinding flower defect in a high-temperature (4000 K) MC simulation. (c) Evolution of the total energy of a similar process in the presence of two other defects (a divacancy and an ad-dimer configuration); in this case, no clear energy barrier is evident. The simulation temperature was 2500 K. (d) Experimental micrographs showing transformations of two grains, one (bottom-left) with nonzero density deficit and another one involving two missing atoms (top) under an electron dose rate of 4.5×10^6 e/(nm^{2}s) for a total exposure time of 240 s with schematic presentations of the structures in clean areas underneath each image. (The complete image sequence is presented as Supporting Information Video 5). Scale bars 1 nm.

step-by-step how a flower defect unwinds under the electron beam. This remarkable transformation has not yet been reported in the literature, despite frequent static observations of the structure itself.[20−23] The stability of the flower defect under most imaging conditions, including our own experimental setup, which was tuned to maximize the bond rotation rate, can be traced to the initial stage of the transformation, which involves two consecutive bond rotations that each increase the energy of the system (by a total of ∼3 eV, according to our DFT calculations (Methods)). Each of the subsequent unwinding steps lowers the total energy of the system until the pristine lattice is reached. Correspondingly, we were able to simulate the disappearance of the flower defect with our MC code only by increasing the simulation temperature (from 2000 to 4000 K) in order to raise the probability for higher-energy states (Figure 4b). (We stress that the temperature has no real physical meaning in the simulations, other than determining the probability for accepting energetically unfavored bond rotations.) Once begun, however, the simulated transformation followed exactly the same path as the one observed experimentally (Figure 4a).

Although the atomic density in graphene grain boundaries is normally identical to that of the hexagonal carbon lattice, we sometimes observed nonzero density deficit in grains and grain boundaries. In Figure 4c we show an example from our simulations in which an initially larger structure first transforms into the flower defect with a nearby divacancy having the V_2(555-777) reconstruction[25] and an adatom pair in the I_2(7557) configuration.[26] Here, the two additional atoms at the GB change the energetics of the transformation process, significantly reducing the energy barrier in comparison to the case presented in Figure 4b.

When a GB loop manifests a density deficit, shrinkage of the interior grain is necessarily accompanied by emission of a vacancy structure, as the excess "volume" must be accommodated somewhere in the graphene lattice; experimental evidence for such an event is presented in the upper part of image sequence Figure 4d. In the lower part of the same sequence, we observe how another grain transforms into the flower defect during observation, in striking resemblance to the simulation presented in Figure 3b. In addition, in the lower right corner of the first panel we see a defect structure

dx.doi.org/10.1021/nl301141g | Nano Lett. 2012, 12, 3168−3173

consisting of a (5|7) dislocation core and two ad-atoms in the I_2(555-777) configuration.[26] These ad-atoms vanish between the first and the second panel, showing that such adatom structures are mobile under our experimental conditions, possibly via the bond rotation mechanism (more frames are available in Supporting Information Video 4). In general, due to the experimental time resolution the role of ad-atoms cannot be completely excluded in other transformations. However, since the total number of atoms in the structures remains constant during observation, except in the rare cases discussed above, their role can hardly be a significant one.

In this study, we have demonstrated that GB migration in graphene can be observed atom-by-atom in real time by utilizing AC-HRTEM, which not only provides atomic-resolution images, but also stimulates bond rotations that in turn induce changes in GB configurations. As anticipated from macroscopic concepts for the energetics of grain boundary migration, we find that these atomic-scale modifications lead to a time-averaged GB translation only in the presence of significant boundary curvature. Moreover, we show that a single graphene grain fully enclosed within another one can even shrink to the point of disappearance, resulting in the restoration of pristine lattice. These findings suggest that graphene may offer the first experimentally accessible platform for in situ atomic-level investigation of a host of GB phenomena, including solute drag, Zener pinning, interaction with other lattice defects and coupling to mechanical stresses.

Methods. *Sample Preparation.* Single and few-layer graphene films were prepared by vacuum-assisted chemical vapor deposition on polycrystalline Cu foils using hexane as a liquid precursor.[27] The Cu foil was heated to 950 °C in the presence of ∼5 mbar of forming gas, Ar-5% H_2, flowing at a rate of ∼400 sccm; the forming gas prevents oxidation of the Cu substrate during annealing. Once the desired temperature was achieved, the Ar/H_2 flow was stopped, and hexane vapor was introduced into the quartz tube under a pressure of 0.5 mbar and a flow rate of ∼4 mL/h, maintaining these conditions for 1 min. Finally, the sample was cooled to room temperature under flowing forming gas at a pressure of ∼5 mbar.

AC-HRTEM Imaging. Aberration-corrected high-resolution (AC-HR)TEM imaging was carried out in an FEI Titan 80−300 transmission electron microscope equipped with an objective-side image corrector. The microscope was operated at 80 kV. The extraction voltage of the field emission source was set to a reduced value of 2 kV in order to minimize the energy spread of the electron beam. The spherical aberration was set to 20 μm, and images were recorded at a Scherzer defocus of approximately −9 nm. Under these conditions, atoms appear dark. The resulting image sequences were background subtracted and drift compensated.[21] Figure 4a shows single exposures, while the others are averaged over 3−10 frames (in which the atomic structure did not change) to improve the signal-to-noise ratio.

Electronic Structure Calculations. Density functional theory (DFT) calculations were carried out with the VASP simulation package,[28] using projector augmented wave potentials[29] to describe core electrons and the generalized gradient approximation[30] to account for exchange and correlation. The flower defect and divacancy models (see Supporting Information) consisted of 200 atoms. For these particular cases, a kinetic energy cutoff of 500 eV was imposed for the plane waves, and a Monkhorst−Pack k-point mesh[31] of 7 × 7 × 1 was employed. Initially created defect configurations were relaxed until atomic forces were below 0.01 eV/Å. The more complex models for estimating the GB energy consisted of 800 atoms. In these cases, the kinetic energy cutoff was set to 300 eV, and a single k-point (Gamma) was used with 0.1 eV/Å as the atomic force convergence criterion in order to reduce the computational expense.

Metropolis Monte Carlo Method. We implemented the MC model so that for each iteration one C−C bond is selected randomly within the simulated graphene structure. After rotation of this bond and complete relaxation of the resulting structure with an analytical model for C−C interactions,[18] the energies of the initial (Γ) and the trial state (Γ′) are compared. The transition Γ → Γ′ is accepted if the following comparison is true

$$u \leq \exp\left(\frac{\Delta E}{k_B T}\right) \quad (1)$$

where $u \in [0, 1]$ denotes a random number, $\Delta E = E - E'$ the energy difference between Γ and Γ′, k_B the Boltzmann constant, and T the simulation temperature. Note that if the energy decreases during the transition ($\Delta E > 0$), the comparison is true, and the trial state is always accepted.

■ ASSOCIATED CONTENT

Supporting Information

Supporting Information contains AC-HRTEM images without overlays, a detailed description of and justification for the Monte Carlo method as well as several AC-HRTEM image sequences parts of which are presented in the figures of the main article. This material is available free of charge via the Internet at http://pubs.acs.org.

■ AUTHOR INFORMATION

Corresponding Author

* E-mail: (J.K.) jani.kotakoski@iki.fi; (U.K.) ute.kaiser@uni-ulm.de.

Present Address

■Department of Physics, University of Vienna, Boltzmanngasse 5, 1090 Vienna, Austria

Author Contributions

¶These authors contributed equally to this work.

Notes

The authors declare no competing financial interest.

●Part of the work was performed during 3 month stays as guest scientists at Ulm University

■ ACKNOWLEDGMENTS

We gratefully acknowledge support by the German Ministry of Science (DFG), Research and the Arts (MWK) of the State of Baden-Wuertternberg within the SALVE (Sub-Angstrom Low-Voltage Electron microscopy) project (U.K., S.K., J.K., O.L., C.E.K.) and the SFB 569 (U.K., S.K., J.K., O.L.) as well as the DFG through the graphene priority programme (V.S., J.S.). Funding was also provided by the Academy of Finland through several projects (A.V.K., J.K., O.L.). J.K., O.L., and A.V.K. thank CSC Finland and PRACE (Project 2011040577) for generous grants of computational resources. S.K. acquired the TEM data. V.S. and J.S. grew the graphene sample and transferred it to TEM grids. J.K. and O.L. designed and carried out the DFT calculations. J.K., O.L., and A.V.K. conceived and designed the MC simulations, and O.L. implemented and executed them.

S.K., J.K., and O.L. analyzed the TEM results, and C.E.K. contributed to understanding and interpreting the results in the context of macroscopic models for GB migration. U.K. supervised the TEM work and assembled the group. All authors participated in the discussion of results and their implications. J.K. wrote the article with the assistance of C.E.K. and all authors commented on the paper.

REFERENCES

(1) Grantab, R.; Shenoy, V. B.; Ruoff, R. S. Anomalous Strength Characteristics of Tilt Grain Boundaries in Graphene. *Science* **2010**, *330*, 946.

(2) Yazyev, O. V.; Louie, S. G. Topological defects in graphene: Dislocations and grain boundaries. *Phys. Rev. B* **2010**, *81*, 195420.

(3) Carlsson, J. M.; Ghiringhelli, L. M.; Fasolino, A. Theory and hierarchical calculations of the structure and energetics of [0001] tilt grain boundaries in graphene. *Phys. Rev. B* **2011**, *84*, 165423.

(4) Yu, Q.; et al. Control and characterization of individual grains and grain boundaries in graphene grown by chemical vapour deposition. *Nat. Mater.* **2011**, *10*, 443−449.

(5) Huang, P. Y.; et al. Grains and grain boundaries in single-layer graphene atomic patchwork quilts. *Nature* **2011**, *469*, 389−392.

(6) An, J.; et al. Domain (Grain) Boundaries and Evidence of "Twinlike" Structures in Chemically Vapor Deposited Grown Graphene. *ACS Nano* **2011**, *5*, 2433−2439.

(7) Kim, K.; et al. Grain Boundary Mapping in Polycrystalline Graphene. *ACS Nano* **2011**, *5*, 2142−2146.

(8) Kotakoski, J.; Krasheninnikov, A. V.; Kaiser, U.; Meyer, J. C. From Point Defects in Graphene to Two-Dimensional Amorphous Carbon. *Phys. Rev. Lett.* **2011**, *106*, 105505.

(9) Kotakoski, J.; et al. Stone-Wales-type transformations in carbon nanostructures driven by electron irradiation. *Phys. Rev. B* **2011**, *83*, 245420.

(10) Kotakoski, J.; Santos-Cottin, D.; Krasheninnikov, A. V. Stability of Graphene Edges under Electron Beam: Equilibrium Energetics versus Dynamic Effects. *ACS Nano* **2012**, *6*, 671−676.

(11) Meyer, J. C.; et al. Accurate measurement of electron beam induced displaced cross sections for single-layer graphene. *Phys. Rev. Lett.* **2012**, *108*, 196102.

(12) Zobelli, A.; Gloter, A.; Ewels, C. P.; Colliex, C. Shaping single walled nanotubes with an electron beam. *Phys. Rev. B* **2008**, *77*, 045410.

(13) Humphreys, F. J.; Hatherly, M. *Recrystallization and Related Annealing Phenomena*, 2nd ed.; Elsevier: Amsterdam, 2004; p 10.

(14) Mølhave, K.; et al. Electron irradiation-induced destruction of carbon nanotubes in electron microscopes. *Ultramicroscopy* **2007**, *108*, 52−57.

(15) Chuvilin, A.; Meyer, J. C.; Algara-Siller, G.; Kaiser, U. From graphene constrictions to single carbon chains. *New J. Phys.* **2009**, *11*, 083019.

(16) Girit, Ç, Ö.; et al. Graphene at the Edge: Stability and Dynamics. *Science* **2009**, *323*, 1705−1708.

(17) Humphreys, F. J.; Hatherly, M. *Recrystallization and Related Annealing Phenomena*, 2nd ed.; Elsevier: Amsterdam, 2004; p 356.

(18) Brenner, D.; et al. A second-generation reactive empirical bond order (REBO) potential energy expression for hydrocarbons. *J. Phys.: Condens. Matter* **2002**, *14*, 783.

(19) Banhart, F.; Kotakoski, J.; Krasheninnikov, A. V. Structural Defects in Graphene. *ACS Nano* **2011**, *5*, 26−41.

(20) Park, H. J.; et al. Growth and properties of chemically modified graphene. *Phys. Status Solidi B* **2010**, *247*, 2915−2919.

(21) Meyer, J. C.; et al. Experimental analysis of charge redistribution due to chemical bonding by high-resolution transmission electron microscopy. *Nat. Mater.* **2011**, *10*, 209−215.

(22) Rutter, G. M.; Crain, J. N.; Guisinger, N. P.; Li, T.; First, P. N.; Stroscio, J. A. Scattering and Interference in Epitaxial Graphene. *Science* **2007**, *317*, 219−222.

(23) Cockayne, E.; et al. Grain boundary loops in graphene. *Phys. Rev. B* **2011**, *83*, 195425.

(24) Westenfelder, B.; Meyer, J. C.; Meyer; Biskupek, J.; Kurasch, S.; Scholz, F.; Krill, C. E., III; Kaiser, U. *Nano Lett.* **2011**, *11*, 5123−5127.

(25) Lee, G. D.; et al. Diffusion, Coalescence, and Reconstruction of Vacancy Defects in Graphene Layers. *Phys. Rev. Lett.* **2005**, *95*, 205501.

(26) Lusk, M. T.; Carr, L. D. Nanoengineering Defect Structures on Graphene. *Phys. Rev. Lett.* **2008**, *100*, 175503.

(27) Srivastava, A.; et al. Novel Liquid Precursor-Based Facile Synthesis of Large-Area Continuous, Single, and Few-Layer Graphene Films. *Chem. Mater.* **2010**, *22*, 3457−3461.

(28) Kresse, G.; Furthmüller, J. Efficient iterative schemes for *ab initio* total-energy calculations using a plane-wave basis set. *Phys. Rev. B* **1996**, *54*, 11169.

(29) Blöchl, P. E. Projector augmented-wave method. *Phys. Rev. B* **1994**, *50*, 17953.

(30) Perdew, J.; Burke, K.; Ernzerhof, M. Generalized gradient approximation made simple. *Phys. Rev. Lett.* **1996**, *77*, 3865.

(31) Monkhorst, H.; Pack, J. Special points for Brillouin-zone integrations. *Phys. Rev. B* **1976**, *13*, 5188.